ACS Catalysis

pubs.acs.org/acscatalysis

Research Article

Enzymatic Δ^1-Dehydrogenation of 3-Ketosteroids—Reconciliation of Kinetic Isotope Effects with the Reaction Mechanism

Michał Glanowski, Patrycja Wójcik, Magdalena Procner, Tomasz Borowski, Dawid Lupa, Przemysław Mielczarek, Maria Oszajca, Katarzyna Świderek, Vicent Moliner, Andrzej J. Bojarski, and Maciej Szaleniec*

Cite This: *ACS Catal.* 2021, 11, 8211−8225

Read Online

ACCESS | Metrics & More | Article Recommendations | Supporting Information

ABSTRACT: Δ^1-Dehydrogenation of 3-ketosteroids catalyzed by flavin adenine dinucleotide (FAD)-dependent 3-ketosteroid dehydrogenases (Δ^1-KSTD) is a crucial step in steroid degradation and synthesis of several steroid drugs. The catalytic mechanism assumes the formation of a double bond in two steps, proton abstraction by tyrosyl ion, and a rate-limiting hydride transfer to FAD. This hypothesis was never verified by quantum-mechanical studies despite contradictory results from the kinetic isotope effect (KIE) reported in 1960 by Jerussi and Ringold [*Biochemistry* **1965**, 4 (10)]. In this paper, we present results that reconcile the mechanistic hypothesis with experimental evidence. Quantum mechanics/molecular mechanics molecular dynamics simulations show that the proposed mechanism is indeed the most probable, but barriers associated with substrate activation (13.4−16.3 kcal·mol^{-1}) and hydride transfer (15.5−18.0 kcal·mol^{-1}) are very close (1.7−2.1 kcal·mol^{-1}), which explains normal KIE values for steroids labeled either at C1 or C2 atoms. We confirm that tyrosyl ion acting as the catalytic base is indeed necessary for efficient activation of the steroid. We explain the lower value of the observed KIE (1.5−3.5) by the nature of the free energy surface, the presence of diffusion limitation, and to a smaller extent, conformational changes of the enzyme upon substrate binding. Finally, we confirm the Ping-Pong bi−bi kinetics of the whole Δ^1-dehydrogenation and demonstrate that substrate binding, steroid dehydrogenation, and enzyme reoxidation proceed at comparable rates.

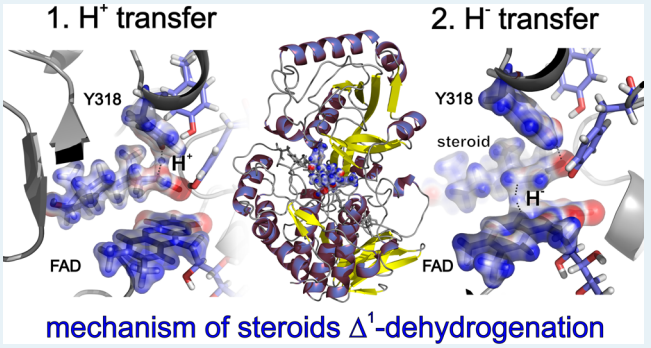

KEYWORDS: *Δ^1-ketosteroid dehydrogenase, 3-ketosteroids, Δ^1-dehydrogenation, kinetic isotope effect, QM/MM, kinetic solvent viscosity effect, Ping-Pong bi−bi mechanism*

INTRODUCTION

Steroids are one of the most important groups of drugs on the market, finding their application in treating inflammation and diseases of immune function, such as allergies, asthma, autoimmune diseases, and several mineral metabolism disorders like hyponatremia, hyperkalemia, osteoporosis, and hypotension as well as in birth control.[1] Glucocorticoids (e.g., dexamethasone) were used in clinical practice and are evaluated as agents for the treatment of acute respiratory distress syndrome, which develops in many patients during infection with SARS-CoV-2.[2] As a result, the value of the global steroid market is expected to reach 17 Bn USD by the end of 2025 with extensive growth predicted in the segment of corticosteroids and anabolic steroids (according to QY Research, Inc.).[3] Steroid drugs are synthesized by a combination of chemical and microbiological methods,[4] where the latter utilizes a natural metabolism of cholesterol or phytosterols in fungi or bacteria. Microbial fermentation very often provides steroid active pharmaceutical ingredients (APIs) that can be further functionalized by chemical or biocatalytic means. One of such biocatalytic processes that has been extensively studied during the last 50 years is Δ^1-dehydrogenation of steroids catalyzed by 56 kDa Δ^1-ketosteroid dehydrogenase (Δ^1-KSTD). Δ^1-KSTDs are essential in the production of several steroid drugs, such as betamethasone,[5,6] boldenone,[7,8] prednisone,[5,9] dexamethasone,[10,11] and steroid APIs [4-androstene-3,17-dione (AD), 1,4-androstadiene-3,17-dione (ADD), and 9α-hydroxy-4-androstene-3,17-dione].[12−14] Due to their high importance in steroid metabolism, and consequently for the pharmaceutical industry, the flavin adenine dinucleotide (FAD)-dependent Δ^1-KSTDs are one of the best-studied steroid-degrading

Received: March 31, 2021
Revised: June 6, 2021
Published: June 20, 2021

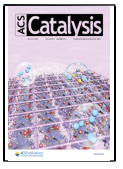

enzymes.[14] They catalyze the regioselective introduction of a double bond between C1 and C2 atoms in ring A of the steroid core (Figure 1).

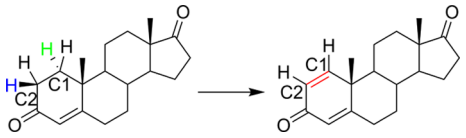

Figure 1. Dehydrogenation of AD catalyzed by Δ^1-KSTD. Abstracted hydrogen atoms, as marked in blue (H2β) and green (H1α), formed a double bond, in red.

The mechanistic hypothesis describing the catalytic mechanism has been formulated based on (i) the structure of only one KSTD from *Rhodococcus erythropolis* (PDB 4c3x and 4c3y),[15,16] (ii) activity tests of genetically modified enzyme variants, and (iii) numerous kinetic studies that yielded values of the kinetic isotope effect (KIE) for chirally labeled substrates.[15,17−21] The currently accepted hypothesis assumes that the overall reaction proceeds according to the Ping-Pong bi−bi mechanism, with the steroid substrate oxidized during reductive half-reaction (RHR) and FAD reoxidation by the electron acceptor during oxidative half-reaction (OHR).[17] RHR proceeds in a step-wise manner, that is, the steroid is activated by the tyrosyl anion, which abstracts the acidic 2β-H proton from the C2 atom with a high degree of stereoselectivity.[20] In the second, supposedly rate-limiting step, 1α hydride is shifted to FAD resulting in the formation of the double bond (Figure 1).[14,22] Surprisingly, this hypothesis was never validated with quantum chemical calculations despite several intriguing results which did not entirely agree with the undoubtedly sensible mechanistic hypothesis. Over 5 decades ago, Jerussi and Ringold provided values of KIEs obtained for steroids selectively labeled with deuterium at C1 and/or C2 positions. The authors observed KIEs for substrates labeled either at C1 or C2 position and the values of V_H/V_D were in the range of 1.2−2.5, which is relatively low for the primary H/D KIE, especially compared to strictly chemical reactions.[21] More importantly, if the second step of RHR indeed was rate-limiting, why was the substitution of 2β protium with deuterium influencing the observed KIE? Another unresolved question concerns the protonation state of Tyr318. As most of the KSTDs exhibit optimum pH under neutral or basic conditions,[17,23,24] it was sensible to assume that it is a tyrosyl ion that deprotonates acidic C2 atom of the steroid. However, several KSTDs have been recently discovered that exhibit optimum activity under slightly acidic conditions, despite highly conserved composition of the active site.[25−27] Therefore, the question is whether the deprotonation of tyrosine is truly necessary for activation of the substrate. We decided to apply advanced multiscale quantum mechanics/molecular mechanics (QM/MM) methods to finally test the mechanistic hypotheses on the reaction mechanism and to try reconciling it with the results of experiments. In this paper, we present a detailed investigation of Δ^1-dehydrogenation of 17-methyl-testosterone (17β-hydroxy-17-methyl-4-androsten-3-one, 17-MT) to metandienone (17β-hydroxy-17-methyl-1,4-androstdien-3-one, MTD), and dihydrotestosterone (17β-hydroxy-5α-androstan-3-one, DHT) to 1-testosterone (17β-hydroxy-5α-androst-1-en-3-one, 1-TE) by Δ^1-KSTD from *R. erythropolis*. We compared possible reaction pathways and calculated values of the intrinsic KIE for the RHR. These results were confronted with kinetic experiments providing proof for the Ping-Pong bi−bi mechanism, including observed KIEs from the competitive, pre- and steady-state kinetic as well as kinetic solvent viscosity effect (KSVE).

METHODOLOGY

Computational Model Setup. The initial atomic coordinates of KSTD from *R. erythropolis* were obtained from Protein Data Bank (PDB ID: 4c3y, resolution 2.3 Å).[15] This crystal structure contains ADD bound in the active site together with the FAD cofactor. ADD was subsequently replaced by 17-MT or by DHT applying the Kabsch method[28] using coordinates of ADD heavy atoms as a template. Protonation states of titratable amino acids were determined using PropKa ver 3.1[29,30] and H++ software[31] at pH = 8, which was reported as optimal for the enzyme activity. According to the predicted pK_a shifts (see the Supporting Information) and after visual inspection of the geometry, it was concluded that Lys450 should be deprotonated, whereas histidine residues number 162, 328, 362, and 408 were protonated at δ positions. The tyrosine in position 318 was considered in a deprotonated state because, according to the mechanistic hypothesis, it serves as a proton acceptor. Missing AMBER parameters for 17-MT, DHT, and tyrosyl anion were obtained at the B3LYP/6-31G(d,p) level of theory in the gas phase with Gaussian16.[32] Point charges were computed using Merz−Kollman electron density calculations[33] and the RESP procedure as implemented in the Antechamber available in AmberTools[34] (see Supporting Information). Parameters for FAD were adapted from RESP ESP charge DDataBase (R.E.DD.B)[35] (see Supporting Information). The systems were neutralized by adding 33 sodium ions in the electrostatically most favorable positions and soaked in a 93.5 × 76.5 × 72.0 Å^3 box with TIP3P[36] water molecules. Models consisting of just the ketosteroid 17-MT and DHT in a 73.5 × 73.0 × 76.2 Å^3 box of TIP3P water molecules were also prepared as reference models in solution.

Classical MD Simulations. The final models (with a total number of 59737 and 59736 atoms for 17-MT and DHT, respectively) were optimized using Amber package[34] with the ff03 force field.[37] After energy minimization and heating from 0 to 303 K over 100 ps with the *NVT* ensemble, the system was equilibrated during 100 ps with *NPT* conditions. Subsequently, *NPT* nonaccelerated and nonbiased molecular dynamic (MD) simulations at 303 K were conducted for 55 ns using periodic boundary conditions. To improve the time of simulations, cutoffs for nonbonding interactions were applied with a value of 8.0 Å. The temperature during the simulations was controlled using the Langevin thermostat.[38] Root mean square deviation (rmsd) indicates that the systems can be considered as equilibrated after 30 ns (see Supporting Information). Conformations during the last 20 ns of simulations were analyzed to obtain representative structures using cluster analysis based on rmsd of positions of heavy atoms of the side chains of Tyr318, Tyr119, Tyr487, and ring A of the 3-ketosteroid and FAD. Geometry closest to the center of the largest cluster was used as the starting structure for QM/MM calculations.[39] For calculations related to the protein-free models, 8 random frames were selected from the last 20 ns of simulation for each ketosteroid.

QM/MM MD Simulations. The QM subsystem consisted of the ketosteroid substrate, the side chain of Tyr318, and a fragment of FAD, as shown in Figure 2, while the rest of the protein and solvent water molecules were represented by

https://doi.org/10.1021/acscatal.1c01479
ACS Catal. 2021, 11, 8211−8225

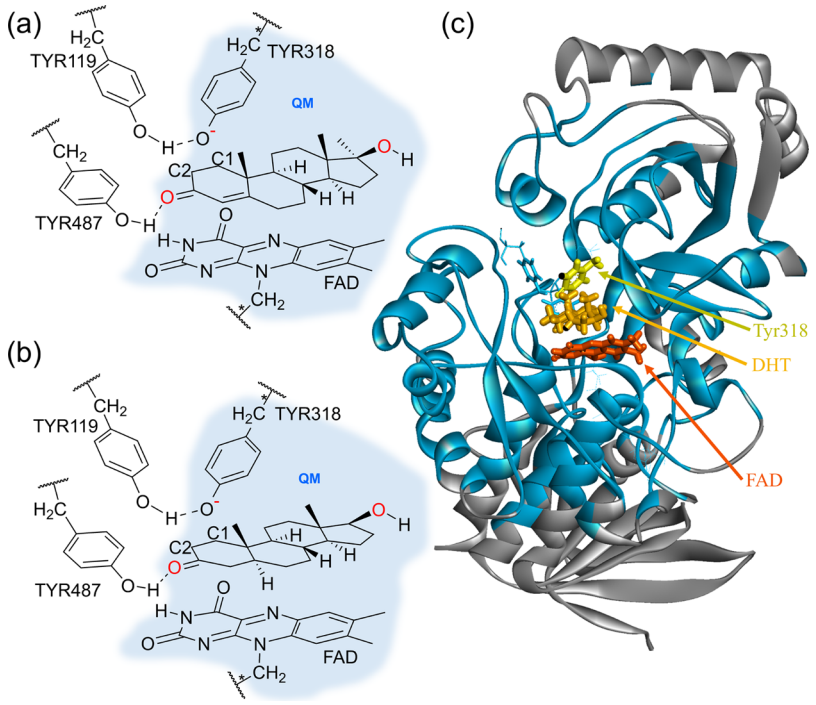

Figure 2. Schematic representation of the active site of the enzyme with substrates: 17-MT (a) and DHT (b). The light blue region contains atoms that are treated quantum mechanically. Quantum link atoms are marked with an asterisk. Overview of the whole model with DHT (c): yellow, orange, and red fragments represent Tyr318, DHT, and FAD, respectively, and flexible part of the model is shown in blue, while the frozen part of the model is in gray. Solvent water molecules are omitted for clarity.

classical AMBER and TIP3P force fields, respectively, as implemented in fDYNAMO library.[40,41] Two hydrogen link atoms[42] were added (Figure 2). Positions of all residues beyond 20 Å from the substrate were fixed. To improve the time of simulations, cutoffs for nonbonding interactions were applied using a smooth switching function between 14.5 and 16 Å. Energies were computed using the standard additive QM/MM scheme. Free energy surfaces (FESs), in terms of potentials of mean force (PMF), were computed for the two chemical steps of the reaction in order to obtain the full free energy profile. The PMFs were computed through the umbrella sampling approach[43] at 303 K.

At first, the potential energy surfaces (PESs) using a selected combination of interatomic distances as a distinguished reaction coordinate were generated. In particular, the antisymmetric combinations of the distances defining the position of the transferred hydrogen, that is, $r_{C2H} - r_{OH}$ for the first step and $r_{C1H} - r_{NH}$ for the second one, were chosen. Then, series of QM/MM MD simulations were carried out in which the distinguished reaction coordinate variable was constrained around the values of the structures generated in the PES with the Umbrella Sampling (US) method,[43] using a parabolic penalty potential with a force constant of 2500 kJ·Å^{-2} mol^{-1}. The values of the variables sampled during the QM/MM simulations were then pieced together to construct a distribution function from which the PMF is obtained using the weighted histogram analysis method.[44] Due to the high computational costs of PMF calculation, the QM Hamiltonian for the QM/MM MD simulations was calculated at the AM1 level of theory. Nevertheless, to reduce the possible errors associated with the semiempirical method, we used an energy spline function defined in terms of interpolated corrections, as described previously.[45] The spline corrections[46] were obtained from single-point calculation at the B3LYP/6-311++G-(2d,2p)/MM level of theory for structures generated along the AM1/MM PESs. Transition state (TS) structures were then fully optimized and characterized at the AM1/MM and B3LYP/6-31G(d,p)/MM level from structures selected from the quadratic region of the FESs. Each of the structures was optimized with the Baker algorithm[47] using the micro−macro iteration scheme.[45] The gradient norm for optimization was maintained lower than 1 kJ·Å^{-1} mol^{-1} level for the QM region and 0.5 kJ·Å^{-1} mol^{-1} for the remaining movable atoms. Every localized TS structure was verified by the existence of one imaginary frequency as computed using the Hessian matrix containing all the coordinates of the QM subsystem in the presence of the MM environment. Intrinsic reaction coordinates were traced down from located TSs to the connecting valleys in mass-weighted Cartesian coordinates, and the vibration analysis was conducted for the ground states to confirm reaching true minima.

Kinetic and Binding Isotope Effects. Averaged KIEs were calculated for the reaction with deuterium-labeled 17-MT and DHT (Figure 3), and individual contributions of each deuteron (i.e., primary or secondary KIE) are presented in the Supporting Information. From the definition of the free energy of a state and using the transition state theory,[48−50] the total partition function and the zero-point energy of light and heavy

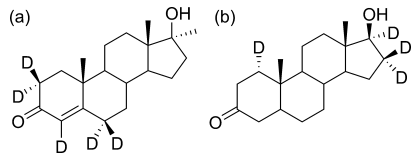

Figure 3. Deuterium-labeled 2,2,4,6,6-d_5-17-MT (a) and 1,16,16,17-d_4-DHT (b) used in the calculations and experiments.

https://doi.org/10.1021/acscatal.1c01479
ACS Catal. 2021, 11, 8211−8225

isotopologues were computed from localized E:S, TS1, E:I, and TS2 structures at the AM1/AMBER and B3LYP/AMBER level of theory, as described elsewhere[51−53] (see Supporting Information). At this point, we must keep in mind the nature of the chemical reactions under study, and quantum tunneling effects could have an impact on the quantitative estimation of the computed activation free energies (reducing the effective barrier) and KIEs (increasing the primary deuterium KIE values). Nevertheless, these possible corrections would not influence the obtained trends, as demonstrated previously.[54,55] Analogically, binding isotope effects (BIE)[56] were calculated from a model of the substrate in a water solution and E:S at the B3LYP/AMBER level of theory. For BIE calculation, the QM region was reduced to the steroid molecule.

EXPERIMENTAL METHODOLOGY

Materials. All chemicals were purchased from Sigma-Aldrich (Germany), Tokyo Chemical Industry (Japan), BioShop (Canada), Carl Roth (Germany), or Chempur (Poland) unless otherwise specified. 4-Androsten-17α-methyl-17β-ol-3-one-2,2,4,6,6-d_5 was purchased from CDN Isotopes (Germany), while 17β-hydroxy-5α-androstan-3-one-1,16,16,17-d_4 was obtained from Alsachim (France).

Protein Expression and Purification. A gene encoding 3-ketosteroid Δ^1-dehydrogenase from *R. erythropolis* (KSTD1) was cloned into a pET15b vector[57] and transformed into calcium chloride chemically competent *Escherichia coli (E. coli)* BL21(DE3)Magic cells (Creative Biolabs). An overnight culture of the transformed cells was grown in 2% (w/v) Lennox Broth (LB) supplemented with 100 μg mL^{-1} ampicillin and 50 μg mL^{-1} kanamycin at 37 °C, 180 rpm. The preculture was diluted a hundred times with 1 L of ampicillin and kanamycin supplemented LB with 0.5 M D-sorbitol and grown under the same conditions as the overnight culture until the OD_{600} reached 0.6. Next, the temperature was reduced to 16 °C, and the culture was induced with 100 μM isopropyl β-D-1-thiogalactopyranoside. After 48 h, the *E. coli* cells were harvested by centrifugation at 4500*g*, 4 °C for 1 h. The cell pellets were resuspended 1:5 (w/v) in the buffer 50 mM Tris-HCl pH 8.5, 100 mM NaCl, 10% (w/v) glycerol, 5 mM β-mercaptoethanol, and 10 mM imidazole and supplemented with 100 μM phenylmethylsulfonyl fluoride. The cell suspension was lysed by sonication (Sonics Vibra-Cell VCX500, 3 s on, 5 s off, 5 min, 40% amplitude, 150 000 J). Cell debris was removed by centrifugation at 40 000*g*, for 1 h at 4 °C. Purification of KSTD was carried out on a 5 mL HisTrap HP (GE Healthcare) column using an FPLC system (BioRad NGC Quest 10 Plus) and linear imidazole gradient 10−300 mM in the previously described buffer. The fractions that absorbed light at a wavelength of 450 nm were collected, desalted by dialysis, and stored at −20 °C. The concentration of the purified active protein was determined using an extinction coefficient of FAD in KSTD 12 627 M^{-1} cm^{-1} at 450 nm.

To determine the KSTD FAD extinction coefficient (ε_{KSTD}), the protein UV−vis spectrum in the range of 650−300 nm was measured (Shimadzu UV-1280) before and after heat denaturation of the sample at 90 °C for 10 min. The concentration of the free FAD was determined spectrophotometrically using ε_{450nm} of 11 300 M^{-1} cm^{-1}. $\Delta\varepsilon_{KSTD}$ was determined spectrophotometrically as a difference between the spectrum of the KSTD with oxidized FAD and the spectrum of the enzyme with the flavoprotein reduced with the excess amount of sodium dithionite under anaerobic conditions (98:2 (v/v) N_2/H_2) divided by the concentration of free FAD. The value of $\Delta\varepsilon_{KSTD}$ at 450 nm equaled 11 368 M^{-1} cm^{-1} and was used to the calculated change in enzyme and substrate concentrations for the global fit of the pre-steady state experiments with 17-MT (see below). The values of ε_{KSTD} for oxidized and reduced KSTD as well as $\Delta\varepsilon_{KSTD}$ in the function of wavelength are provided in the Supporting Information.

Protein MS-Based Identification. 100 μg of KSTD was precipitated with 6-excess of cold acetone and resuspended in 20 μL of 0.5 M triethylammonium bicarbonate buffer with the addition of 2% SDS solution. Then, the protein was reduced by tris-(2-carboxyethyl)-phosphine and alkylated with iodoacetamide. Finally, the protein was digested by 2 μg of Trypsin Gold (from Promega) and desalted on MacroSpin Columns with the C18 resin obtained from The Nest Group, Inc. The obtained peptide maps were evaporated to dryness in a vacuum centrifuge (Labconco). Prior to the nanoLC-MS/MS analysis, the peptides were resuspended in 20 μL of 0.1% formic acid. Nanochromatography combined with tandem mass spectrometry analysis (nanoLC-MS/MS) used to separate protein digests was performed using the Proxeon nanocapillary chromatography system controlled by the Hystar software (Bruker Daltonics). Separations were performed using a PepMap column (15 cm long, 75 μm ID, C18, 3 μm particle size, 100 Å pore size, Thermo-Scientific). The gradient was formed using H_2O/0.1% HCOOH (A) and ACN/0.1% HCOOH (B) at a flow rate of 300 nL/min. A gradient was formed from 2 to 35% B at 50 min and up to 90% B at 55 min and then kept until 65 min at 90% B. Fractions eluted from the column were directly deposited with an α-cyano-4-hydroxycinnamic acid matrix on a MALDI target plate by a Proteineer fc II sample collector (Bruker Daltonics). Fifteen-second fractions were collected, 96 fractions for one sample, and spotted on 384 MALDI target plate. The mass spectrometry analyses were performed on ultrafleXtreme (Bruker Daltonics) in positive ion mode.

The acquired mass spectra were analyzed using the Bruker Data Analysis 4.0 software (Bruker Daltonics) and were identified using the Mascot 2.4.1 algorithm (Matrix Science) against the NCBInr protein sequence database ver. 2012. Search parameters were set in the following way: taxonomy: all entries; modification: carbamidomethyl (fixed) or methionine dioxidation (variable); up to 1 missed cleavage; peptide charges: +1; and mass tolerance: 25 ppm for precursor mass and 0.6 Da for fragment mass. Proteins with at least two fragmented, unique peptides detected were considered, and an additional criterion was an ion score higher than 40, which is above the level of false positives ($p \leq 0.05$).

Spectrophotometric Activity Assay. Values of kinetic constants were obtained using a stopped-flow approach. Single wavelength kinetic traces were recorded on the SX20 (Applied Photophysics, UK) stopped-flow spectrophotometer with a 10 mm pathlength and photomultiplier detector. The data were collected and processed using Pro-Data software. All measurements were conducted at 30 °C. The temperature in the stopped-flow experiments was controlled by a Labo Plus (Polyscience, Poland) thermostat bath. Solutions were treated with argon for several minutes to provide anaerobic conditions. All reported concentrations are the final values obtained after mixing and dilution of the reactants. All collected data were

https://doi.org/10.1021/acscatal.1c01479
ACS Catal. 2021, 11, 8211−8225

processed using OriginPro 2019b software or Octave for global fit.[58]

Steady-State Kinetics. A typical reaction mixture contained 50 mM Tris-HCl buffer pH 8.0, 6.3 nM of KSTD, and varying concentrations of 2,6-dichloroindophenol (DCPIP; 0.025−0.1 mM) and AD (5−120 μM) in isopropanol (the final concentration 1%). In each measurement, one glass syringe of the stopped-flow instrument was filled with the solution of AD and DCPIP and the second one with the enzyme and DCPIP solution. Kinetic traces were followed at 700 nm ($\varepsilon_{700[\text{pH 8.0}]}$ = 5100 M^{-1} cm^{-1}). The initial rate constants were obtained by fitting a linear function to the first 10 s of the studied reaction. Subsequently, the received data were fitted to the nonsequential Ping-Pong bi−bi model with a nonlinear regression and to an alternate model (e.g., sequential model). The model was selected based on statistical parameters such as R^2, χ^2, AICc, and errors of estimated constants.

Pre-Steady-State Kinetics. The K_D and k_{cat} values for 17-MT were determined in the reaction of 7.1 μM of KSTD with the 17-MT (concentration 25 to 200 μM) using 50 mM Tris-HCl at pH 8.0. In each measurement, one glass syringe of the stopped-flow instrument was filled with the solution of the steroid dissolved in dioxane/buffer solution (the final dioxane concentration 5%), while the second one contained the enzyme solution in the buffer. The reaction was conducted under anaerobic conditions at 30 °C. The kinetics of FAD reduction was followed at 450 nm for 31.25 ms. The obtained traces (8 repetitions for each 17-MT concentration) were globally fitted to a kinetic model (a set of differential equations) consisting of two consecutive reversible steps: formation/dissociation of the ES complex (k_1 and k_{-1}) and FAD reduction/oxidation by the substrate/product (k_2 and k_{-2}): ES ⇌ E'P. To assess the information content of the set of traces and to estimate confidence intervals for fitted kinetics constants, confidence contours on error maps were determined at the level by 10% higher than the minimum determined from unconstrained fitting.[59] Least-squares fitting and confidence contour calculations were performed with an in-house written Octave script,[58,60] which is deposited together with the fitted data at Mendeley Data.[61] A more complicated—three-step model, which included an additional equilibrium (ES ⇌ EI) between substrate binding and the redox step, was also fitted, yet the confidence contours unequivocally showed that thus determined k_1 and k_{-1} are unconstrained by the data and can attain arbitrarily high values. The E + S ⇌ ES ⇌ E'P model was also fitted to the data obtained during the KSVE experiment, but due to lack of enough data for enzyme saturated with the substrate, it was not possible to unequivocally determine k_1 and k_{-1} values.

Kinetic Solvent Viscosity Effect. The KSVE was determined by pre-steady-state kinetics measurements using either glycerol or polyethyleneglycol (PEG) 20000 as viscosigen. The reaction mixture contained 50 mM Tris-HCl buffer pH 8.0, 8.9 μM of KSTD, and varying concentrations of AD (50−200 μM) in 2-methoxyethanol (EGME; the final concentration 5%) and glycerol (at a concentration of 0.27, 1.27, and 2.27 M) or PEG 20000 [at a concentration of 4.2 and 10% (w/v)]. In each measurement, one glass syringe of the stopped-flow instrument was filled with the solution of steroid and the other one with the enzyme solution. The kinetic traces were followed at 450 nm for 35 to 125 ms. The obtained traces were fitted with single exponential functions

$$A = A_0 e^{-\lambda t} + y_0 \quad (1)$$

where λ is the observed decay rate (eigenvalue) of the flavin reduction.

Afterward, the collected data were fitted to the Michaelis−Menten model with nonlinear regression.

The dynamic viscosity of reaction mixtures was determined using the rolling-ball Lovis 2000 M/ME viscometer supplied by Anton Paar at 30 °C. For this purpose, a short capillary tube and a 1.59 mm diameter steel ball were used.

In order to match the hydrodynamic diameter of PEG to that of the KSTD enzyme, the diffusion coefficients of PEG 4000; PEG 8000; PEG 20000 and KSTD were measured in 50 mM Tris-HCl buffer pH 8.0 at 30 °C using the Zetasizer Nano ZS apparatus (Malvern Instruments). Measurements were carried out at a 173° scattering angle using a frequency-doubled diode-pumped solid-state 532 nm laser as an incident light source. Knowing the diffusion coefficient of the molecules, their hydrodynamic diameters (d_H) were calculated using the Stokes−Einstein relationship

$$d_H = \frac{k_B T}{3\pi\eta D} \quad (2)$$

where k_B is the Boltzmann constant, T is the absolute temperature, η is the dynamic viscosity of the medium, and D is the diffusion coefficient of the molecule.

Kinetic Isotope Effect. The KIE at C1 and C2 atoms of the 3-ketosteroid core were determined by a direct method under steady-state or pre-steady-state conditions or in competition experiments for DHT and 17-MT, respectively.

Steady-State Kinetics. The reaction velocities were determined in a spectrophotometric activity assay using a UV-2700 spectrophotometer (Shimadzu) in 0.5 mL quartz cuvettes with a 10 mm path length at 30 °C. The measurements were carried out in 50 mM Tris-HCl buffer pH 8.0 with 200 μM DCPIP, 200 μM steroid dissolved in dioxane [2% (v/v)], and 84.4 nM of KSTD. The reduction of DCPIP was followed at 700 nm ($\varepsilon_{700[\text{pH 8.0}]}$ = 5100 M^{-1} cm^{-1}). All measurements were performed in triplicates. The initial rate constants were obtained with linear regression fitted to the initial parts of the kinetic curves.

Pre-Steady-State Kinetics. λ_{obs} for C1 was determined in the reaction of 8.9 μM KSTD with either 100 μM DHT or 1,16,16,17-d_4-DHT in EGME/buffer solution (10%). λ_{obs} for the C2 atom was measured with 7.1 μM KSTD and either 250 μM 17-MT or 2,2,4,6,6-d_5-17-MT analogue dissolved in dioxane/buffer solution (6%). Each experiment was repeated at least 12 times. The obtained traces were fitted with single exponential functions, and the ratio of the average $\lambda_{obsH}/\lambda_{obsD}$ was determined.

Competition Experiment. The $^D(V/K)$ kinetic isotope method was measured according to the protocol described previously.[62,63] The determination of the competitive $^D(V/K)$ KIE was based on the fractions of the converted light (x_1) and heavy (x_2) substrate according to the formula

$$^D\left(\frac{V}{K}\right) = \frac{k_1}{k_2} = \frac{\log(1 - x_1)}{\log(1 - x_2)} \quad (3)$$

$^D(V/K)$ was established by a nonlinear fit in Origin 2019 from the reformulated function of $x_1(x_2)$

$$x_1 = 1 - (1 - x_2)^{k_1/k_2} \quad (4)$$

https://doi.org/10.1021/acscatal.1c01479
ACS Catal. 2021, 11, 8211−8225

The reactions were carried out in triplicates and the reaction mixtures consisted of 50 mM Tris-HCl buffer pH 8.0, 100 μM DCPIP, equal 100 μM amounts of substrates and their deuterated homologues (17-MT and 2,2,4,6,6-d_5-17-MT or DHT and 1,16,16,17-d_4-DHT) in EGME (the final concentration 2%), and KSTD (0.4 nM for 17-MT or 0.9 nM for DHT). The reactions were run under anaerobic conditions [98:2 (v/v) N_2/H_2] at 30 °C for 18 min. The conversion of each substrate was analyzed with LC-ESI-MS/MS (Agilent 1290 Infinity System equipped with an MS Agilent 6460 Triple Quad Detector) using the positive single-ion monitoring mode (303.3, 308.3, 301.3, and 305.3 m/z signals for $[M + H]^+$ of 17-MT, 2,2,4,6,6-d_5-17-MT, MTD, and 2,4,6,6-d_4-MTD as well as 291.3, 295.3, 289.3, and 292.3 m/z for $[M + H]^+$ of DHT, 1,16,16,17-d_4-DHT, 1-TE, and 16,16,17-d_3-1-TE). The separation was carried out on the Agilent Zorbax Eclipse Plus C18 column (2.1 × 50 mm, 1.8 μm) using the ACN/H_2O/HCOOH (40:60:0.1, v/v) mobile phase in the isocratic mode with a flow rate of 0.4 mL/min, 30 °C, and 1 μL injection volume (see Supporting Information for details of the MS method) The quantitation of analytes was conducted using external calibration based on commercial standards or products synthesized by 100% enzymatic conversion of the standards.

RESULTS AND DISCUSSION

Kinetic Mechanism. Our kinetic experiments confirmed that Δ^1-dehydrogenation catalyzed by 3-Δ^1-KSTD is indeed proceeded according to the Ping-Pong bi−bi mechanism (Figure 4), as previously observed for transhydrogenation by Itagaki et al.[17]

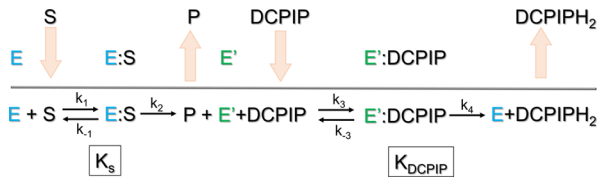

Figure 4. Schematic representation of the nonsequential Ping-Pong bi−bi mechanism.[64−66] K_S and K_{DCPIP} are dissociation constants of complexes E:S and E':DCPIP, respectively. k_2 and k_4 represent k_{cat} for RHR and OHR, respectively.

The steroid substrate (S) binds to the enzyme (E), then it is oxidized, and the dehydrogenated product (P) is released (RHR). Subsequently, the reduced enzyme (E′) binds to an electron acceptor (DCPIP). $FADH^-$ gets oxidized, and reduced $DCPIPH_2$ is released (OHR). The obtained kinetic data for different DCPIP concentrations were fitted to three types of the two-substrate reaction mechanism equations describing sequential random bi−bi, sequential ordered bi−bi, or nonsequential Ping-Pong bi−bi mechanism. The goodness of the fit was assessed by the comparison of the statistical parameters. Because R^2 values do not reflect the best fit for nonlinear models with a different number of parameters, model discrimination was also based on the Akaike information criterion (AICc parameter)[67] with smaller AICc values indicating a better agreement with kinetic data. The nonsequential Ping-Pong mechanism can be described by the following equation

$$V = \frac{V_{max}[S][DCPIP]}{K_S[DCPIP] + K_{DCPIP}[S] + [S][DCPIP]} \quad (5)$$

where V_{max} is equal to $k$catPing-Pong$[E_t]$. Kinetic parameters are provided in Table 1.

Table 1. Kinetic Parameters Obtained from Data Fitted to the Nonsequential Ping-Pong bi−bi Mechanism Model

S	K_S [μM]	K_{DCPIP} [μM]	V_{max} [μM min^{-1}]	$k_{cat}^{Ping\text{-}Pong}$ [s^{-1}]
AD	119.6 ± 16.3	40.2 ± 6.9	181.1 ± 17.3	479.1 ± 45.8

RHR mechanism investigation.

We started the analysis of the RHR with pre-steady-state kinetics conducted for 17-MT and global fit of the kinetic data with the simple RHR model assuming reversibility of both steps

$$E + S \underset{k_{-1}}{\overset{k_1}{\rightleftharpoons}} E{:}\ I \underset{k_{-2}}{\overset{k_2}{\rightleftharpoons}} E{:}\ P \quad (6)$$

As a result, we were able to estimate values of the kinetic constants (Table 2) describing binding (k_1) and release of the substrate as well as a composite kinetic constant describing jointly two steps of the RHR reaction in the direction of substrate oxidation (k_2) or the reverse direction of substrate reduction (k_{-2}). The ratio of k_{-1} to k_1 yields K_D of 96.7 μM, which is half of the estimated K_D value for AD, indicating a higher affinity of KSTD1 for 17-MT (see Table 3). More important, however, is the fact that the rate of E:S formation is of the same magnitude as the chemical step (k_2 422 s^{-1}), exceeding it only above substrate concentration of 46 μM. This result indicates that any process slowing down the substrate binding (such as diffusion or hindrance of the environment to the conformational change of the enzyme upon enzyme binding) can influence the observed reaction velocity.

Table 2. Kinetic Parameters Obtained from Global Data Fitted to the Pre-Steady-State Experiment with 17-MT

	constant value	stdd	10% confidence range
k_1 [s^{-1} μM^{-1}]	9.0	0.1	6.9−12.3
k_{-1} [s^{-1}]	872	12	676−1259
k_2 [s^{-1}]	422	1.3	327−593
k_{-2} [s^{-1}]	98.2	0.4	77−129

Table 3. Pre-Steady-State Kinetic Parameters for Dehydrogenation of AD at Different Viscosities Introduced by Glycerol (Microviscosity) or PEG 20000 (Macroviscosity)

η [mPa s]	K_D [μM]	k_2 [s^{-1}]	k_2/K_D [M−1 s−1]
	Glycerol		
1.006 (η0)	227.7 ± 13.9	658.4 ± 23.6	(2.9 ± 0.2) × 10^6
1.283	331.2 ± 22.9	571.2 ± 26.3	(1.7 ± 0.1) × 10^6
1.671	339.5 ± 15.0	379.7 ± 11.2	(1.1 ± 0.1) × 10^6
	PEG 20000		
1.011 (η0)	208.0 ± 13.7	533.4 ± 20.0	(2.6 ± 0.2) × 10^6
2.711	210.5 ± 12.2	374.4 ± 12.6	(1.8 ± 0.1) × 10^6
7.636	348.9 ± 31.2	337.9 ± 19.8	(1.0 ± 0.1) × 10^6

In pursuit of an explanation of the low KIE observed for KSTDs by us (see below) and Jerussi and Ringold,[21] and in the light of these results, we decided to evaluate to what extent a substrate diffusion into the enzyme active site or the enzyme conformational change occurring upon substrate binding can

https://doi.org/10.1021/acscatal.1c01479
ACS Catal. 2021, 11, 8211−8225

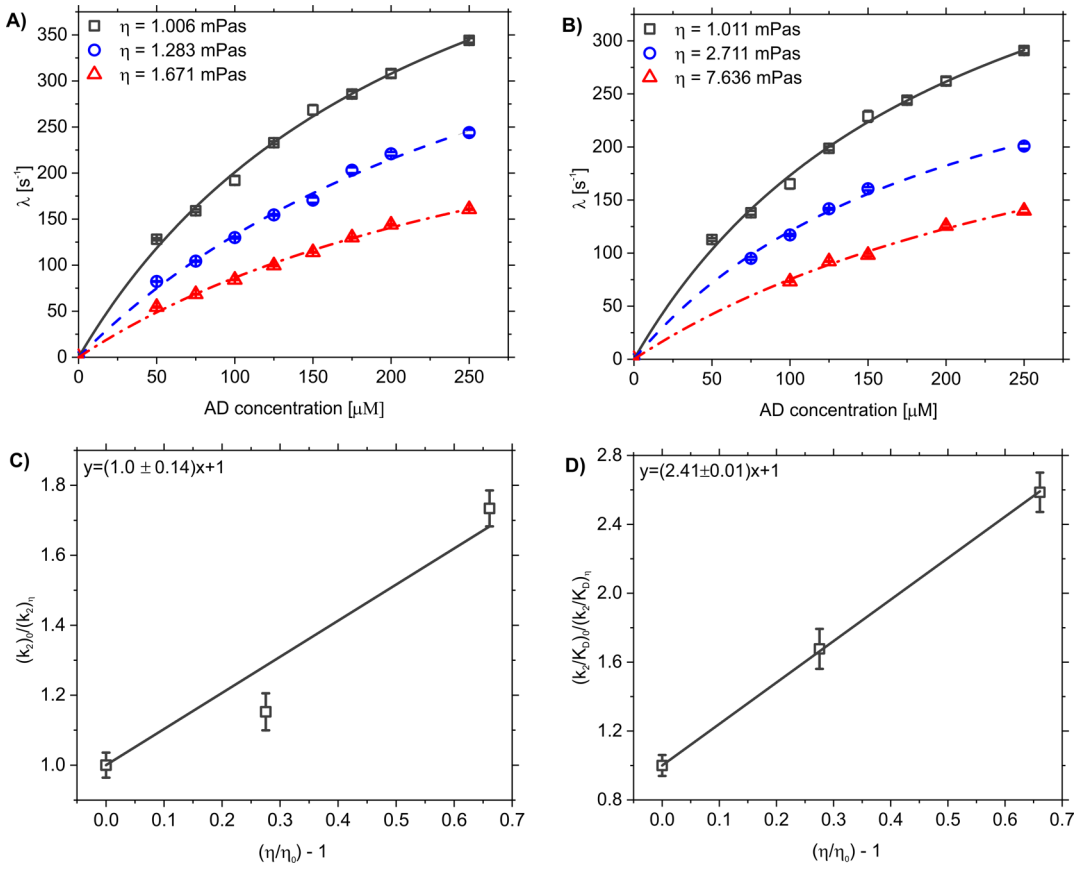

Figure 5. Effect of solvent viscosity on the pre-steady-state kinetics parameters for KSTD with AD as a substrate (A) Michaelis−Menten model fitting kinetics in glycerol, (B) Michaelis−Menten model fitting kinetics in PEG 20 000, (C) effect on the k_2 value in glycerol, (D) effect on the k_2/K_D value in glycerol (see Supporting Information for figures with PEG). Reaction conditions: 50 mM Tris-HCl buffer pH 8.0 with 8.9 μM of KSTD, 50−250 μM of AD in EGME (6%) and 0.27 M (□), 1.27 M (□) or 2.27 M (△) glycerol (A) or 0% (□), and 4.2% (□) or 10% (△) glycerol PEG 20000 (B), respectively.

affect the kinetic parameters. To address this, we measured the KSVE.[68] The KSVE was determined by rapid mixing of the enzyme with AD under anaerobic conditions in the stopped-flow spectrophotometer. The measurements were carried out at 30 °C using glycerol or PEG 20000 as a viscosigens providing micro- or macroviscosity, respectively. The effect of substrate concentration on the net decay rate of flavin reduction (λ) at increasing glycerol or PEG 20000 concentration is shown in Figure 5. λ can be described by eq 7[69]

$$\lambda = \frac{k_2[S]}{K_D + [S]} \tag{7}$$

where k_2 is the limiting rate of FAD reduction under saturation conditions ([S]≫[E]) and K_D is the dissociation constant of the enzyme−substrate complex. Over the microviscosity range of 1.006−1.671 mPa s, we observed a statistically significant decrease of k_2 (from 658 to 407 s^{-1}) and an increase of the K_D values (from 224 to 372 μM). The obtained data were displayed in a plot of the normalized kinetic parameter: $(k_2)_0/(k_2)_\eta$ and $(k_2/K_D)_0/(k_2/K_D)_\eta$, (Figure 5) as a function of relative viscosity $(\eta/\eta_0 - 1)$, and then, the linear function was fitted with the intercept fixed at 1.[68] The value of the linear slope determines the degree of dependence of the normalized kinetic parameters on viscosity. The slope of the line in the plot presented in Figure 5C is 1.0 ± 0.14 and indicates that the process catalyzed by KSTD strongly depends on solution microviscosity. Meanwhile, in the experiment with PEG 20000, the slope of the line in the plot presented in the Supporting Information is only 0.12 ± 0.05, which indicates minuscule dependence of the catalytic step from the macroviscosity introduced by PEG. Therefore, we can conclude that there is no significant conformational change of the protein during the reaction.

In the case of the plot of $(k_2/K_D)_0/(k_2/K_D)_\eta$ *versus* $(\eta/\eta_0 - 1)$, for glycerol, the slope was >2 (see Figure 5D), which suggests that the formation of the enzyme−substrate complex is also viscosity-dependent and may be partially limited by diffusion. As the experiment with PEG on $(k_2/K_D)_0/(k_2/K_D)_\eta$ yielded the slope of 0.26 ± 0.01, we concluded that the conformational change of the enzyme upon binding is only slightly limited by macroviscosity introduced by PEG and the binding is predominantly limited by the diffusion of the substrate.

In a separate experiment, we have confirmed that glycerol has no inhibitory effect on the enzyme (data not shown).

The conclusions drawn from KSVE are in agreement with the analysis of the MD simulations conducted for the study. In particular, we did not observe any significant changes in the enzyme conformation upon substrate binding. However, our MD simulations might not have been long enough to describe such a conformational change, and such phenomena were not the focus of this paper.

https://doi.org/10.1021/acscatal.1c01479
ACS Catal. 2021, 11, 8211−8225

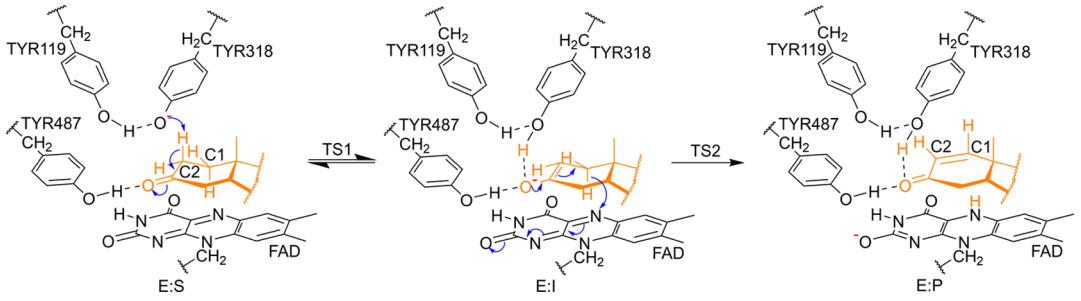

Figure 6. Reaction scheme of dehydrogenation of DHT. The substrate is marked in orange, and dashed lines represent hydrogen bond interactions. The first step corresponds to the abstraction of the 2β proton at the C2 position of ketosteroid by tyrosine anion Tyr 318 and the second step is the 1α hydride transfer from the C1 position of the substrate to the N5 atom of the FAD.

The complementary kinetic studies conducted for AD with the steady-state or pre-steady-state technique enabled the comparison of the eigenvalues associated with those two phases.

The k_2 estimated from the rate of FAD reduction (RHR) with AD was in the range of 533−658 s^{-1} (depending on the enzyme batch, Table 3), while $k_{cat}^{Ping\text{-}Pong}$ from steady-state reaction with AD and DCPIP was 479.1 ± 45.8 s^{-1}. The k_2 turns out to be even higher (604−742 s^{-1}) if the kinetic results from the pre-steadystate experiment are extrapolated to the same viscosity as that measured for the reaction mixture used in the steady-state experiment (η_{H2O} = 0.896 mPa s). As values of extrapolated k_2 and $k_{cat}^{Ping\text{-}Pong}$ were obtained under different conditions, it is very difficult to directly compare their values. However, if one analyzes the relationship between $k_{cat}^{Ping\text{-}Pong}$, k_2, and k_4, (eq 8), then one can see that k_2 and k_4 should be of the same order of magnitude.

$$k_{cat}^{Ping\text{-}Pong} = \frac{k_2 k_4}{k_2 + k_4} \tag{8}$$

Modeling of the Reaction Mechanism. To test the mechanistic hypothesis for Δ^1-dehydrogenation of 3-ketosteroids by KSTD with deprotonated Tyr318, we first computed QM/MM PESs describing the two process, that is, (i) the abstraction of a proton from C2 by Tyr318 and (ii) the hydride transfer from C1 to FAD, as presented in the Supporting Information. The minimum energy pathway from the reactants (E:S) to products (E:P) leads through the formation of a carbanionic intermediate (E:I) (Figure 6). According to the topology of the PES, a process involving the simultaneous transfer of both hydrogen atoms does not exist. The alternate reaction pathway starting with a hydride transfer also turns out to be extremely unlikely due to the very high energy of the carbocation intermediate (see Supporting Information). Therefore, the formation of the carbanion by proton transfer from C2 is the only thermodynamically possible way to start a reaction. This route leads to the currently accepted mechanism. Then, the FESs were computed in terms of PMFs to obtain the free energy profile of the full reaction. This procedure allowed us to describe the RHR process, as summarized in Figure 7. Analysis of the initial enzyme−substrate complex (E:S) shows how the substrate is localized in the active site pocket with its ring A almost parallel to the isoalloxazine ring system of FAD. The steroid position is stabilized by H-bonds between the 3-keto group and Tyr487 as well as Gly491. Tyr318 anion is interacting by an H-bond with Tyr119. These H-bonds remain stable throughout the whole RHR. In the first step of the reaction, the steroid is activated by the abstraction of the proton from the 2β position by the Tyr318 anion. Then, when the enolate intermediate is formed (E:I), a new H-bond is created between the 3-keto group and Tyr318 protonated with 2β-H atom. Formation of the intermediate enolate results in a change in the ring A geometry and repositioning of the substrate in the active site, which decreases the distance between 1αH of the substrate and $N5_{FAD}$ atom in E:I. This change of geometry facilitates the next step of the reaction, when the hydride is transferred from the 1α position of the ketosteroid to N5 atom in the FAD residue, resulting in a two-electron-reduced (hydroquinone) unprotonated state of flavin. Finally, the double bond is formed between C1 and C2 atoms of the steroid and the enzyme−product complex is formed (E:P). The resulting FESs obtained for the reaction with DHT (blue line) and 17-MT (orange line) are shown in Figure 8.

The general trend of the FESs obtained for both molecules is similar, that is, the higher barrier is associated with hydride transfer which corresponds to TS2, with free energy barriers of 18.0 and 16.3 kcal·mol^{-1} for DHT and 17-MT, respectively. Both formed intermediates are 3.3 and 2.8 kcal·mol^{-1} less stable than E:S of DHT and 17-MT, respectively. Both TS1 and TS2 barriers are lower for 17-MT than for DHT (13.4 and 15.5 kcal·mol^{-1} *vs* 16.3 and 18.0 kcal·mol^{-1}, respectively for TS1 and TS2). A detailed description of the calculated reaction mechanism with full distances and geometry analysis is available in Supporting Information. As can be deduced from the FESs, the enolate is quite well stabilized, being only a few kcal·mol^{-1} above the free energy of the enzyme−substrate complex. In contrast to previous assumptions, the free energy barriers for the first and second steps are comparable. Besides that, however, this mechanism is in line with the widely accepted hypothesis. The mutational studies described by Rohman et al.[15] provided useful clues about the mechanism. Replacing Tyr318 with Phe rendered the enzyme completely inactive, while Y119F and Y487F mutants retained only trace activities (0.05 and 2.6% of original activity, respectively). The experimental data suggest that these tyrosines are crucial for enzyme reactivity. Our QM/MM modeling confirmed the role of both residues. Tyr487 takes part in the binding of the ketosteroid during the whole reaction and stabilizes its activated intermediate by a hydrogen bond. Meanwhile, Tyr119 interacts with Tyr318 anion with a hydrogen bond, and this interaction also remains stable throughout the whole RHR. The Tyr318 anion acts as a base that abstracts a proton from the substrate. Surprisingly, after protonation, it becomes a hydrogen bond donor to the intermediate product, similarly to Tyr487 that interacts with the keto group of the steroid.

https://doi.org/10.1021/acscatal.1c01479
ACS Catal. 2021, 11, 8211−8225

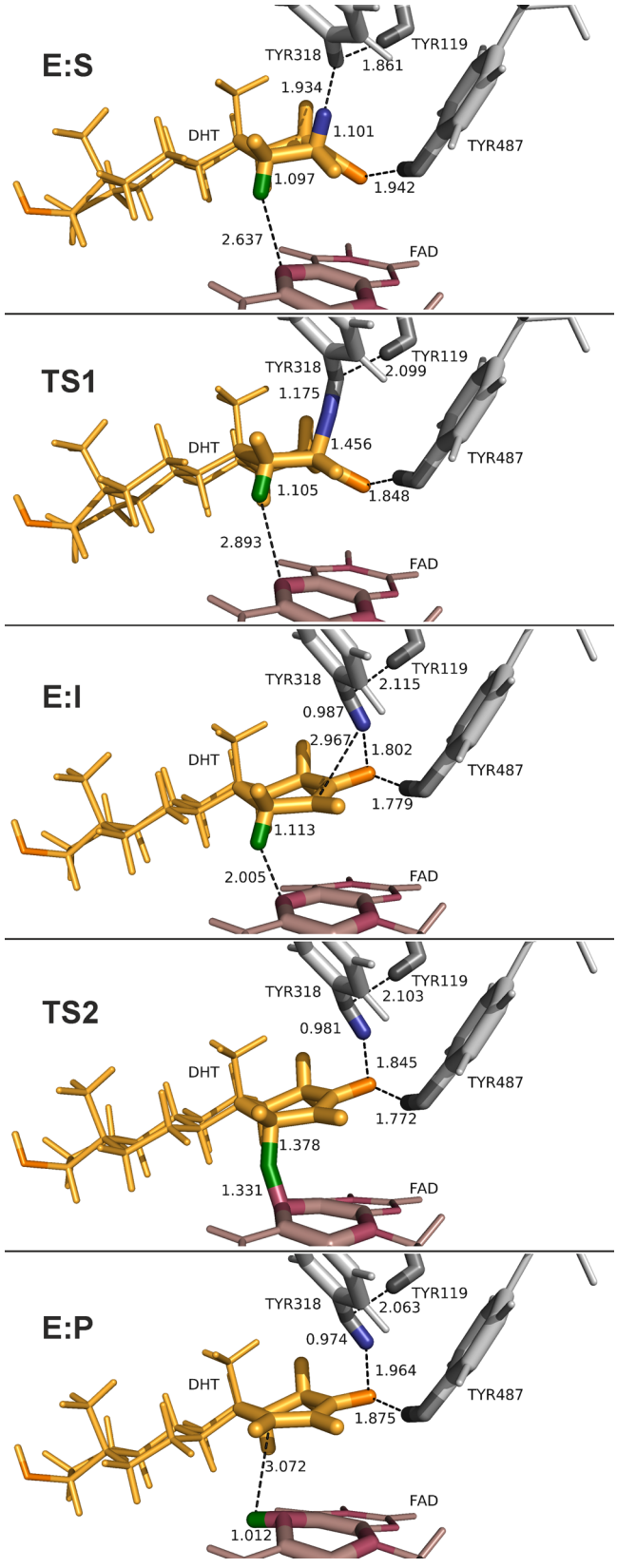

Figure 7. Details of the active site of representative structures of the key-states located along the Δ^1-dehydrogenation of DHT. The distances are given in Å. The transferring atoms are in blue and green.

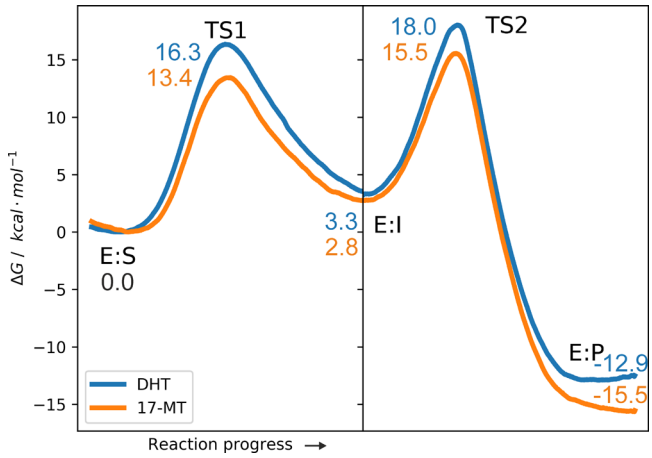

Figure 8. FESs of Δ^1-dehydrogenation of 17-MT (orange line) and DHT (blue line). Results obtained at B3LYP/6-311++g-(2d,2p):AM1/AMBER level of theory at 303 K.

Therefore, Tyr318 does not only acts as a catalytic base activating the C−H bond in the first step of the reaction but also stabilizes the intermediate enolate. This fact can explain the residual activity of the Y487F, as Tyr318 can stabilize the carboanion intermediate. Up to date, this role was attributed solely to stabilization by H-bond formed by the 3-keto group, Tyr487 and Gly491.[15] A similar situation was postulated for Δ^5-3-ketosteroid isomerase where ketosteroid homoenolate is stabilized by low barrier hydrogen bonds.[70] Finally, the average Mulliken and ChelpG charges confirm that the second step occurs via hydride transfer, leading to the formation of $FADH^-$ (see population analysis deposited in the Supporting Information).

Most of the KSTDs catalyze reaction at neutral to basic pH, which supports the hypothesis of the presence of the tyrosyl ion in the active site. However, some reports indicate that the Δ^1-dehydrogenation can proceed under mild acidic conditions,[25,27] and there were no unequivocal proofs for the deprotonated state of Tyr318. Therefore, we investigated a possible alternative mechanism with protonated Tyr318. However, preliminary results indicate that the potential energies of the first TS and intermediate are extremely high (44.8 and 27.9 kcal·mol^{-1}, respectively); therefore, an alternative mechanism with protonated Tyr318 can be discarded. A detailed description of this alternative pathway is available in Supporting Information.

KIEs and BIEs. The values of KIE were initially estimated with a steady-state technique using 200 μM concentrations of steroids and DCPIP, following the method used by Jerussi and Ringold.[21] Such experiments yielded values of KIE of 1.49 ± 0.04 and 1.28 ± 0.02 for DHT and 17-MT, respectively. As our preliminary stopped-flow analysis indicated that the enzyme reoxidation may influence the result of the experiment, we also collected KIEs using the pre-steady-state technique, recording directly the reduction of FAD. Although we have not observed an increase of the KIE for 17-MT, which was calculated as the ratio of $\lambda_{obs}{}^{H}/\lambda_{obs}{}^{D} \approx k_2{}^{H}/k_2{}^{D}$ and equaled 1.5 ± 0.04 (see Supporting Information), we measured a significantly higher value for C1-substituted DHT, where the $k_2{}^{H}/k_2{}^{D}$ ratio was 3.5 ± 0.04.

To gain further insight into the effect of binding to the active site of the enzyme of the labeled substrates on KIE, we measured the $^{D}(V/K)$ in the competition experiment. The obtained values were 2.2 ± 0.02 for 17-MT and 2.4 ± 0.07 for DHT, indicating that in the case of DHT, the binding

https://doi.org/10.1021/acscatal.1c01479
ACS Catal. 2021, 11, 8211−8225

Table 4. Theoretical QM/MM (B3LYP/AMBER) and Experimental Values of KIEs Obtained for Deuterium-Labeled 17-MT and DHT[a]

	theoretical KIE ± SE	experimental KIE ± SE		
		direct pre-steady-state	competitive $^{D}(V/K)$	direct steady-state
	17-MT/2,2,4,6,6-*d*5-17-MT			
E:S → TS1	5.39 ± 0.04			
E:I → TS1	5.13 ± 0.02	1.5 ± 0.04	2.2 ± 0.02	1.28 ± 0.02
E:I → TS2	0.92 ± 0.02			
E:S → TS2	0.98 ± 0.01			
	DHT/1α,16,16,17-d_4-DHT			
E:S → TS1	1.12 ± 0.01			
E:I → TS1	0.97 ± 0.01	3.5 ± 0.04	2.4 ± 0.07	1.5 ± 0.04
E:I → TS2	4.36 ± 0.05			
E:S → TS2	4.95 ± 0.05			

[a]Theoretical values of KIE were computed for each possible individual step of the reaction. The values of direct pre-steady-state KIE correspond to the ratio of the observed λ value (see eq 7); values of direct steady-state KIE correspond to the ratio of activities measured in standard activity assay (200 μM DCPIP/steroid); and $^{D}(V/K)$ values were obtained with a competition method.

decreases the observed KIE. Surprisingly, we observed a slight increase of the KIE for 17-MT when measured in a competitive experiment compared to a direct measurement method. These results indicate that we can expect an inverse BIE for DHT and a normal (above 1) effect for 17-MT.

To address this issue, we calculated BIE at the B3LYP/AMBER level of theory, obtaining values of 0.97 ± 0.06 and 0.76 ± 0.05, respectively, for DHT and 17-MT. As the values of the calculated BIE were lower than unity for both substrates, we can conclude that under simulation conditions, deuterated substrates are bound better by the enzyme than the non-deuterated ones. These predictions are in qualitative agreement only in the case of DHT.

We should underline that in our MD simulation, we model a limit case, where the substrate is either in complex with enzyme or in pure water. However, steroids are so hydrophobic that it is not possible to dissolve them in pure water in concentrations enabling the saturation of KSTD1 (100−200 μM). In our experiments, the addition of the organic solvent was used (5% dioxane or 10% EGME), which stabilized the substrate in the solution by providing thermodynamically favorable hydrophobic interactions. Therefore, the experimental BIEs should be closer to unity than those predicted in our modeling, and we cannot exclude the possibility of even normal (i.e., above 1) BIE for 17-MT.

We assume that the qualitative agreement of our BIE prediction for DHT with results of V_{max} and V/K KIE stems from the difference in the deuteration pattern between 2,2,4,6,6-d_5-17-MT and 1,16,16,17-d_4-DHT. In the case of 17-MT, the deuteron labels are in ring A or B, which are bound inside the enzyme, while in the case of DHT, three deuterons are located on the ring D, which is exposed to the solvent (see Supporting Information). As a result, the environment of the DHT deuterons changes only in the case of the C1 substituent, while for the rest of the deuterons, the situation remains unchanged (no difference between solvent and enzyme−substate complex). In consequence, the lack of organic solvent in the simulation will strongly influence the estimation of BIE for 17-MT, while only a small effect will be expected for DHT.

Generally, KIE experiments are in agreement with our estimation of k_2 and k_4. The kinetic assay, based on the process of DCPIP reduction (k_4), is less sensitive to isotope labels, which results in lowering of the observed KIE (i.e., partial masking the intrinsic KIE).

Our experimental KIE results obtained for KSTD from *R. erythropolis* are similar to those reported by Jerussi and Ringold.[21] They performed a series of KIE measurements using KSTD from *B. sphaericus* with 5α-3-keto- and Δ^4-3-ketosteroids deuterated at 1α and 2β positions. Surprisingly, it was found that substitutions at any of these positions affected the V_{max}. Substantial values of KIE were observed mostly for 1α substitution (V_{maxH}/V_{maxD} = 1.9) and much lower for 2β (V_{maxH}/V_{maxD} = 1.2−1.3) in the case of 5α-3-keto steroids. However, in the case of ketosteroid with an additional double bond in ring A (i.e., Δ^4-3-ketosteroids), both substitutions, at 1α or 2β, affected the observed kinetic rate (V_{maxH}/V_{maxD} = 2.4−2.5). Values obtained for 1α and 2β substitutions were too high to be explained by the secondary isotope effect.

To understand this unusual effect we conducted a series of KIE calculations based on QM/MM optimized geometries of E:S, TS1, E:I, TS2, and E:P for 17-MT and DHT. Results of KIEs derived from calculations and experiments are shown in Table 4.

For the Δ^1-dehydrogenation of DHT, isotopic substitutions at 1α should strongly affect the hydride transfer (TS2) but have an almost negligible influence on the proton transfer (TS1). On the other hand, the experiments showed that substitutions at each position (i.e., C1 or C2) affected the kinetics of the RHR and the whole reaction. Such behavior could be explained with an unknown mechanism where both hydrogens are transferred simultaneously, and what would be observed was primary KIE for both substituted positions. This hypothesis was, however, discarded as experimental data,[20,21] and results from our calculations show that hydrogen atoms are removed in a step-wise manner. Another potential explanation of the experimental values would be a situation where the barrier heights of TS1 and TS2 were so close, that both of them affected the reaction rate.[21] As it turns out, our QM/MM free energy profile of the most favorable mechanism combined with calculations of intrinsic KIE confirms this hypothesis (see Figure 8). Finally, the overall value of KIE can be further decreased by binding and other non-chemical steps (e.g., conformational changes of the protein, diffusion limitation of reagents, as demonstrated by KSVE), but for qualitative analysis, we will focus only on the influence of reaction profile and intrinsic KIEs to the overall KIE. The studied reaction is taking place according to the following reaction scheme (9)

https://doi.org/10.1021/acscatal.1c01479
ACS Catal. 2021, 11, 8211−8225

$$\text{E: S} \underset{k_{\text{I-S}}}{\overset{k_{\text{S-I}}}{\rightleftharpoons}} \text{E: I} \xrightarrow{k_{\text{I-P}}} \text{E: P} \tag{9}$$

Due to the high barrier between the products and the intermediate (see Figure 8), a reverse process from products to the intermediate (E:P to E:I) can be considered negligible. Then, the expression for k_2 would be

$$k_2 = \frac{k_{\text{S-I}} k_{\text{I-P}}}{k_{\text{S-I}} + k_{\text{I-S}} + k_{\text{I-P}}} \tag{10}$$

Using eq 10, it is possible to analyze the contribution of each kinetic constant to the overall KIE. We will use the following notation

$$\text{KIE}_{\text{i}} = \frac{k_{\text{i}}^{\text{H}}}{k_{\text{i}}^{\text{D}}} \tag{11}$$

where KIE_{i} is the KIE associated with an individual step characterized by kinetic constant k_{i} (i = S−I, I−S, I−P). KIEs on the k_2 value would be as follows (derivation is given in Supporting Information)

$$\text{KIE}_2 = \text{KIE}_{\text{S-I}}\text{KIE}_{\text{I-P}} \cdot \frac{\frac{1}{\text{KIE}_{\text{S-I}}} + \frac{1}{\text{KIE}_{\text{I-S}}}\frac{k_{\text{I-S}}^{\text{H}}}{k_{\text{S-I}}^{\text{H}}} + \frac{1}{\text{KIE}_{\text{I-P}}}\frac{k_{\text{I-P}}^{\text{H}}}{k_{\text{S-I}}^{\text{H}}}}{1 + \frac{k_{\text{I-S}}^{\text{H}}}{k_{\text{S-I}}^{\text{H}}} + \frac{k_{\text{I-P}}^{\text{H}}}{k_{\text{S-I}}^{\text{H}}}} \tag{12}$$

Then, according to eq 12, KIE_2 is a function of 5 variables: $\text{KIE}_{\text{S-I}}$, $\text{KIE}_{\text{I-P}}$, $\text{KIE}_{\text{I-S}}$, $k_{\text{I-S}}^{\text{H}}/k_{\text{S-I}}^{\text{H}}$, and $k_{\text{H-P}}^{\text{H}}/k_{\text{S-I}}^{\text{H}}$. Three of these variables can be obtained based on the results of QM/MM calculations ($\text{KIE}_{\text{S-I}}$, $\text{KIE}_{\text{I-P}}$, $\text{KIE}_{\text{I-S}}$). For further analysis, we set a range of 10^{-3} to 10^{3} for both ratios $k_{\text{I-S}}^{\text{H}}/k_{\text{S-I}}^{\text{H}}$ and $k_{\text{I-P}}^{\text{H}}/k_{\text{S-I}}^{\text{H}}$. These ratios were estimated from the free energy profiles and Eyring equation. Nevertheless, we have to bear in mind that such values are subject to some error. It is also possible to replace $k_{\text{I-S}}^{\text{H}}/k_{\text{S-I}}^{\text{H}}$ and $k_{\text{I-P}}^{\text{H}}/k_{\text{S-I}}^{\text{H}}$ in eq 12 by a function of free energies

$$\log \frac{k_{\text{i}}}{k_{\text{S-I}}} = \frac{\Delta G_{\text{S-I}}^{\ddagger} - \Delta G_{\text{i}}^{\ddagger}}{\ln(10)RT} \tag{13}$$

As a result, KIE_{obs} can be analyzed as a function of $\text{KIE}_{\text{S-I}}$, $\text{KIE}_{\text{I-P}}$, $\text{KIE}_{\text{I-S}}$, $\Delta GS\_I^{\ddagger} - \Delta G_{\text{I-S}}^{\ddagger}$, and $\Delta G_{\text{S-I}}^{\ddagger} - \Delta G_{\text{I-P}}^{\ddagger}$.

Taking into account the above mentioned considerations, we can plot maps of all possible values of KIE_2 for 17-MT and DHT (Figure 9). Black curves correspond to the values of KIE measured in our experiments (with confidence bands based on the experimental standard error of the mean for KIE estimation). Centers of white circles represent KIE_2 values calculated from QM/MM results: 1.09 for 17-MT and 4.78 for DHT. These circles have a radius of 1 kcal·mol^{-1} error (the error of the applied theoretical method) which translates to the confidence ranges of KIE for 0.97−2.0 and 3.31−5.0, respectively for 17-MT and DHT. As can be seen in the plots in Figure 9, the curves representing the experiments for both substrates intersect with the circles corresponding to QM/MM values. It is easy to notice that both circles represent wide ranges of KIE values. Thus, in a mechanism like this one, it is necessary to estimate free energies with very small errors to obtain an accurate theoretical prediction of KIE_{obs}, combined with experiments capable of measuring KIEs also with high accuracy. Nevertheless, a fair agreement between theoretical results and experiment can be found, even without considering other factors that may lead to a decrease of measured KIE.

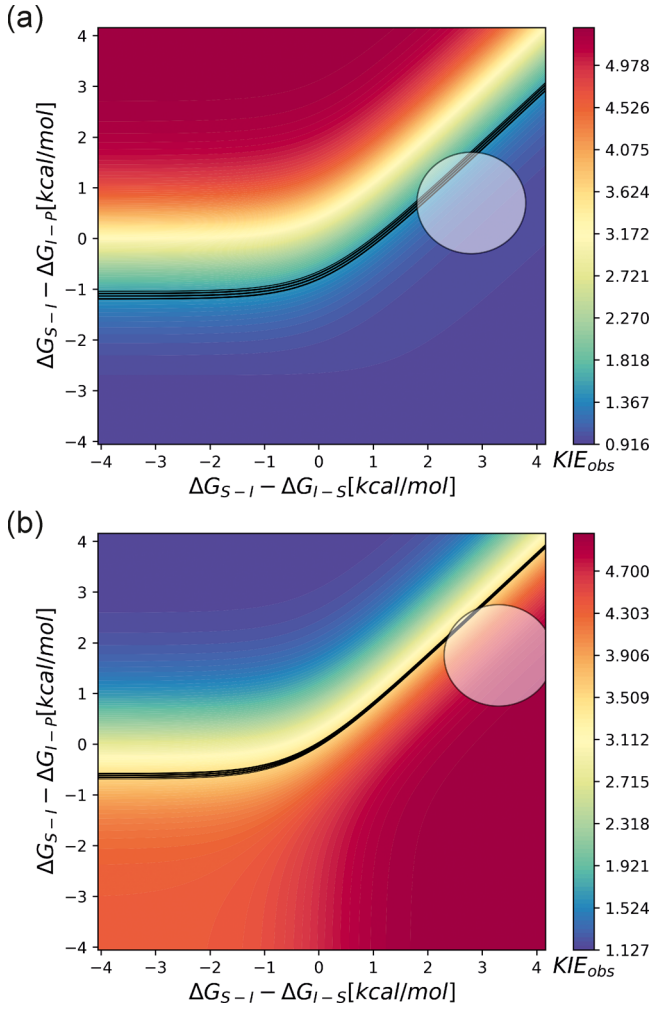

Figure 9. Maps of possible KIE values for 17-MT (a) and DHT (b) as a function of the difference in energy barriers. Black curves represent experimental values (with additional lines indicating experimental errors), and white circles represent the calculated QM/MM KIEs (with 1 kcal·mol^{-1} radius, as the error associated with the method).

Our analysis demonstrated that only the energy landscape of our mechanism can reconcile the experimental KIE results obtained for substitutions at both C1 and C2 positions, which both lead to KIE values significantly greater than one but much lower than the calculated intrinsic KIE. The main reason for this phenomenon is the relation between individual rate constants leading to a situation where both steps have a significant influence on the overall process.

CONCLUSIONS

The reaction catalyzed by Δ^1-KSTD from *R. erythropolis* was investigated using QM/MM computational methods and experimental kinetic measurements of isotope effects. We first proved that dehydrogenation proceeds via a two-step Ping-Pong bi−bi mechanism, which is in line with the widely accepted hypothesis.[16,17] Calculations performed from two different initial states of the enzyme, one with Tyr318 as a tyrosyl anion and the second for a protonated Tyr318, allow us to conclude that the existence of deprotonated tyrosine is essential for initializing the Δ^1-dehydrogenation process. We

https://doi.org/10.1021/acscatal.1c01479
ACS Catal. 2021, 11, 8211−8225

have shown that the enolate intermediate is stabilized not only by Tyr487 and Gly491 but also by Tyr318. This role of Tyr318 was not reported up to date, but it is in agreement with previous mutational studies revealing the complete inactivation of the enzyme after replacing this residue. However, the retention of minimal activity of the Y487F mutant may indicate that Tyr318 can take over the stabilizing role of Tyr487.[15]

Despite the general agreement with previously proposed mechanisms for the reaction catalyzed by Δ^1-KSTD, the free energy barriers for the first and second steps deduced from our QM/MM simulations turned out to be comparable. This result appears to be at the origin of the surprising KIEs which seemed to contradict the mechanistic hypothesis for over half a century. Our computational results derived from the exploration of the FESs and calculations of BIE and intrinsic KIE, finally explained why deuterium substitution affects the overall reaction rate, regardless of the labeled position. This is the effect of comparable free energy barriers for the first and second step. The difference is so small, that both steps influence the overall reaction rate. Our experimental values of KIE obtained for KSTD1 are consistent with those described for the enzyme from *B. sphaericus*, although we were able to demonstrate that the KIE measured in the pre-steady-state at C1 is significantly higher than the value obtained in the steady-state experiment. Therefore, the conclusions seem to be generally applicable to the whole class of Δ^1-KSTD. Furthermore, we are convinced that our holistic approach to describing enzyme kinetics by experimental (steady- and pre-steady-state kinetics, KIE, and KSVE) and theoretical methods (QM/MM MD, global fit to kinetics, and analysis of potential crossing points of theory and experiments) applies to any enzymatic system and provides a potential guideline for elucidation of similar problems. We also pointed out potential pitfalls which may lead to discrepancies in modeling and experiment due to the influence of additives used to introduce the organic substrate into the assay. Quantitative agreement between computational and experimental results is nontrivial to achieve because, as can be seen from the relationship between k_2, K_D, and viscosity, the relative values of k_1, k_2, and k_4, diffusion-controlled processes and, to smaller effect, conformational changes upon binding, as well as reoxidation of the enzyme play important roles in the overall reactivity of KSTD. Despite these obstacles, however, the application of complementary techniques can lead to a better understanding of the enzymatic mechanism, which has eluded scientists for over 50 years.

■ ASSOCIATED CONTENT

Supporting Information

The Supporting Information is available free of charge at https://pubs.acs.org/doi/10.1021/acscatal.1c01479.

PDB files of representative structures optimized at the B3LYP/AMBER level of theory and cartesian coordinates of TS (ZIP)

Population analysis and coordinates of all stationary structures from the main reaction pathway (XLSX)

Details on the modeling methodology and analytical LC−MS/MS procedure, a detailed description of the mechanisms, derivation of equations, details on enzyme identification (SDS PAGE, proteomics) and kinetics (figures for Ping-Pong bi−bi fit, KSVE for PEG 20000, pre-steady-state, V_{max} and $^{D}(V/K)$ KIE), results of DLS for KSTD and PEG, Cartesian coordinates of TSes, details on the calculation of KIE (per atom contributions) and Wigner tunneling corrections, figures depicting binding mode of deuterated 17-MT and DHT (PDF)

■ AUTHOR INFORMATION

Corresponding Author

Maciej Szaleniec − *Jerzy Haber Institute of Catalysis and Surface Chemistry, Polish Academy of Sciences, 30-239 Krakow, Poland;* orcid.org/0000-0002-7650-9263; Email: maciej.szaleniec@ikifp.edu.pl

Authors

Michał Glanowski − *Jerzy Haber Institute of Catalysis and Surface Chemistry, Polish Academy of Sciences, 30-239 Krakow, Poland*

Patrycja Wójcik − *Jerzy Haber Institute of Catalysis and Surface Chemistry, Polish Academy of Sciences, 30-239 Krakow, Poland*

Magdalena Procner − *Jerzy Haber Institute of Catalysis and Surface Chemistry, Polish Academy of Sciences, 30-239 Krakow, Poland*

Tomasz Borowski − *Jerzy Haber Institute of Catalysis and Surface Chemistry, Polish Academy of Sciences, 30-239 Krakow, Poland;* orcid.org/0000-0002-3450-3576

Dawid Lupa − *Jerzy Haber Institute of Catalysis and Surface Chemistry, Polish Academy of Sciences, 30-239 Krakow, Poland*

Przemysław Mielczarek − *Laboratory of Proteomics and Mass Spectrometry, Maj Institute of Pharmacology, Polish Academy of Sciences, 31-343 Krakow, Poland*

Maria Oszajca − *Faculty of Chemistry, Jagiellonian University, 30-387 Krakow, Poland;* orcid.org/0000-0003-2690-0085

Katarzyna Świderek − *Department of Physical and Analytical Chemistry, Universitat Jaume I, 12071 Castellón, Spain;* orcid.org/0000-0002-7528-1551

Vicent Moliner − *Department of Physical and Analytical Chemistry, Universitat Jaume I, 12071 Castellón, Spain;* orcid.org/0000-0002-3665-3391

Andrzej J. Bojarski − *Department of Medicinal Chemistry, Maj Institute of Pharmacology, Polish Academy of Sciences, 31-343 Krakow, Poland;* orcid.org/0000-0003-1417-6333

Complete contact information is available at: https://pubs.acs.org/10.1021/acscatal.1c01479

Author Contributions

M.G. conducted all calculations under MSz. V.M. and K.Ś. supervised, analyzed results, developed discussion, co-authored the main text, edited text, and created figures. P.W. overexpressed and purified KSTD, conducted experiments with the KSVE effect and KIE, co-authored methods and results section, edited text, and created figures. M.P. conducted steady-state kinetic experiments and co-authored the method section. P.M. conducted proteomic analysis and co-authored methods. D.L. conducted viscosity and DLS experiments and co-authored methods and results/Supporting Information sections. T.B. developed Octave scripts and conducted global-fit of 17-MT kinetics, M.O. supervised pre-steady-state kinetic experiments and edited text. K.Ś. and V.M. supervised

https://doi.org/10.1021/acscatal.1c01479
ACS Catal. 2021, 11, 8211−8225

calculation, provided funding, co-authored method section, and edited text. A.B. co-supervised M.G., provided funding, and edited text. M.S. designed the project, planned the research, acquired funding, and supervised. M.G., P.W., and M.P. analyzed experimental and modeling data, co-authored the main text, and edited text.

Notes

The authors declare no competing financial interest.

■ ACKNOWLEDGMENTS

The authors acknowledge partial financial support from the National Science Centre Poland under the OPUS grant number UMO-2016/21/B/ST4/03798. M.G and P.W. acknowledge the fellowship with project no. POWR. 03.02.00-00-I013/16. This research was supported in part by PLGrid (CYFRONET) Infrastructure, by the Spanish Ministerio de Ciencia e Innovación (grant PGC2018-094852-B-C21 and PID2019-107098RJ-I00), the Generalitat Valenciana (grant AICO/2019/195 and SEJI/2020/007) and Universitat Jaume I (grant UJI·B2020-031 and UJI-A2019-04). We acknowledge the joint consortium "Interdisciplinary Centre of Physical, Chemical and Biological Sciences" of ICSC PAS and INP PAS for providing access to the Agilent 1290 Infinity System with an automatic autosampler and an M.S. Agilent 6460 Triple Quad Detector.

■ ABBREVIATIONS

Δ^1KSTD, Δ^1-ketosteroid dehydrogenase; 17-MT, 17-methyltestosterone, 17β-hydroxy-17-methyl-4-androsten-3-one; DHT, dihydrotestosterone, 17β-hydroxy-5α-androstan-3-one; DCPIP, 2,6-dichloroindophenol; AD, 4-androsten-3,17-dione; RHR, reductive half reduction; FES, free energy surface; qm/mm, quantum mechanics/molecular mechanics; md, molecular dynamics

■ REFERENCES

(1) Ericson-Neilsen, W.; Kaye, A. D. Steroids: Pharmacology, Complications, and Practice Delivery Issues. *Ochsner J.* **2014**, *14*, 203−7.
(2) Solinas, C.; Perra, L.; Aiello, M.; Migliori, E.; Petrosillo, N. A Critical Evaluation of Glucocorticoids in the Management of Severe COVID-19. *Cytokine Growth Factor Rev* **2020**, *54*, 8−23.
(3) Global Steroids Industrial Chain Market Growth Overview and Forecast b. 2021, https://www.qyresearch.com/index/detail/701226/global-steroids-industrial-chain-market (accessed Feb 05, 2021).
(4) Fernández-Cabezón, L.; Galán, B.; García, J. L. New Insights on Steroid Biotechnology. *Front. Microbiol.* **2018**, *9*, 958.
(5) James, P.; Rolls, A. Dehydrogenation of Corticoids without Side Chain Degradation by Septomyxa. U.S. Patent 4,088,537 A, May 9, 1978.
(6) Spelling, T. Process for the Overexpression of Dehydrogenases. U.S. Patent 7,416,866 B2, Aug 26, 2008.
(7) Chen, M.-M.; Wang, F.-Q.; Lin, L.-C.; Yao, K.; Wei, D.-Z. Characterization and application of fusidane antibiotic biosynethsis enzyme 3-ketosteroid-Δ1-dehydrogenase in steroid transformation. *Appl. Microbiol. Biotechnol.* **2012**, *96*, 133−142.
(8) Mao, S.; Wang, J.-W.; Liu, F.; Zhu, Z.; Gao, D.; Guo, Q.; Xu, P.; Ma, Z.; Hou, Y.; Cheng, X.; Sun, D.; Lu, F.; Qin, H.-M. Engineering of 3-ketosteroid-Δ1-dehydrogenase based site-directed saturation mutagenesis for efficient biotransformation of steroidal substrates. *Microb. Cell Factories* **2018**, *17*, 141.
(9) Costa, S.; Zappaterra, F.; Summa, D.; Semeraro, B.; Fantin, G. Δ1-Dehydrogenation and C20 Reduction of Cortisone and Hydrocortisone Catalyzed by Rhodococcus Strains. *Molecules* **2020**, *25*, 2192.
(10) Arthur, N. Process for Production of Dienes by Corynebacteria. U.S. Patent 2,837,464 A, June 3, 1958.
(11) Herráiz, I. Chemical Pathways of Corticosteroids, Industrial Synthesis from Sapogenins. *Methods Mol. Biol.* **2017**, *1645*, 15−27.
(12) Donova, M. V. Transformation of Steroids by Actinobacteria: A Review. *Appl. Biochem. Microbiol.* **2007**, *43*, 1−14.
(13) Donova, M. V.; Egorova, O. V. Microbial Steroid Transformations: Current State and Prospects. *Appl. Microbiol. Biotechnol.* **2012**, *94*, 1423−1447.
(14) Rohman, A.; Dijkstra, B. W. The role and mechanism of microbial 3-ketosteroid Δ1-dehydrogenases in steroid breakdown. *J. Steroid Biochem. Mol. Biol.* **2019**, *191*, 105366.
(15) Rohman, A.; Van Oosterwijk, N.; Thunnissen, A.-M. W. H.; Dijkstra, B. W. Crystal Structure and Site-directed Mutagenesis of 3-Ketosteroid Δ1-Dehydrogenase from Rhodococcus erythropolis SQ1 Explain Its Catalytic Mechanism. *J. Biol. Chem.* **2013**, *288*, 35559−35568.
(16) Dijkstra, B. W.; van Oosterwijk, N.; Rohman, A. Structure and Catalytic Mechanism of 3-Ketosteroid Dehydrogenases. *Procedia Chem.* **2016**, *18*, 3−11.
(17) Itagaki, E.; Matushita, H.; Hatta, T. Steroid Transhydrogenase Activity of 3-Ketosteroid-δ-Dehydrogenase from Nocardia corallina. *J. Biochem.* **1990**, *108*, 122−127.
(18) Hayano, M.; Ringold, H. J.; Stefanovic, V.; Gut, M.; Dorfman, R. I. The Stereochemical Course of Enzymatic Steroid 1,2-Dehydrogenation. *Biochem. Biophys. Res. Commun.* **1961**, *4*, 454−459.
(19) Levy, H. R.; Talalay, P. Bacterial Oxidation of Steroids. *J. Biol. Chem.* **1959**, *234*, 2014−2021.
(20) Ringold, H. J.; Hayano, M.; Stefanovic, V. Concerning the Stereochemistry and Mechanism of the Bacterial C-1,2 Dehydrogenation of Steroids. *J. Biol. Chem.* **1963**, *238*, 1960−1965.
(21) Jerussi, R.; Ringold, H. J. The Mechanism of the Bacterial C-1,2 Dehydrogenation of Steroids. III. Kinetics and Isotope Effects*. *Biochemistry* **1965**, *4*, 2113−2126.
(22) Ringold, H. J.; Gut, M.; Hayano, M.; Turner, A. Contribution to the Steric Course of Steroid Reduction and Dehydrogenation. *Tetrahedron Lett.* **1962**, *3*, 835−837.
(23) Shao, M.; Sha, Z.; Zhang, X.; Rao, Z.; Xu, M.; Yang, T.; Xu, Z.; Yang, S. Efficient androst-1,4-diene-3,17-dione production by co-expressing 3-ketosteroid-Δ1-dehydrogenase and catalase inBacillus subtilis. *J. Appl. Microbiol.* **2017**, *122*, 119−128.
(24) Itagaki, E.; Wakabayashi, T.; Hatta, T. Purification and characterization of 3-ketosteroid-Δ1-dehydrogenase from Nocardia corallina. *Biochim. Biophys. Acta, Protein Struct. Mol. Enzymol.* **1990**, *1038*, 60−67.
(25) Wojtkiewicz, A. M.; Wójcik, P.; Procner, M.; Flejszar, M.; Oszajca, M.; Hochołowski, M.; Tataruch, M.; Mrugała, B.; Janeczko, T.; Szaleniec, M. The efficient Δ1-dehydrogenation of a wide spectrum of 3-ketosteroids in a broad pH range by 3-ketosteroid dehydrogenase from Sterolibacterium denitrificans. *J. Steroid Biochem. Mol. Biol.* **2020**, *202*, 105731.
(26) Tataruch, M.; Wójcik, P.; Wojtkiewicz, A. M.; Zaczyk, K.; Szymańska, K.; Szaleniec, M. Application of Immobilized Cholest-4-en-3-one Δ1-Dehydrogenase from Sterolibacterium Denitrificans for Dehydrogenation of Steroids. *Catalysts* **2020**, *10*, 1460.
(27) Chiang, Y.-R.; Ismail, W.; Gallien, S.; Heintz, D.; Van Dorsselaer, A.; Fuchs, G. Cholest-4-En-3-One-Δ 1 -Dehydrogenase, a Flavoprotein Catalyzing the Second Step in Anoxic Cholesterol Metabolism. *Appl. Environ. Microbiol.* **2008**, *74*, 107−113.
(28) Kabsch, W. A discussion of the solution for the best rotation to relate two sets of vectors. *Acta Crystallogr., Sect. A: Found. Crystallogr.* **1978**, *34*, 827−828.
(29) Søndergaard, C. R.; Olsson, M. H. M.; Rostkowski, M.; Jensen, J. H. Improved Treatment of Ligands and Coupling Effects in Empirical Calculation and Rationalization of pKa Values. *J. Chem. Theory Comput.* **2011**, *7*, 2284−2295.

https://doi.org/10.1021/acscatal.1c01479
ACS Catal. 2021, 11, 8211−8225

(30) Olsson, M. H. M.; Søndergaard, C. R.; Rostkowski, M.; Jensen, J. H. PROPKA3: Consistent Treatment of Internal and Surface Residues in Empirical pKa Predictions. *J. Chem. Theory Comput.* **2011**, *7*, 525−537.
(31) Anandakrishnan, R.; Aguilar, B.; Onufriev, A. V. H++ 3.0: Automating pK Prediction and the Preparation of Biomolecular Structures for Atomistic Molecular Modeling and Simulations. *Nucleic Acids Res.* **2012**, *40*, W537−W541.
(32) Frisch, M. J.; Trucks, G. W.; Schlegel, H. B.; Scuseria, G. E.; Robb, M. A.; Cheeseman, J. R.; Scalmani, G.; Barone, V.; Petersson, G. A.; Nakatsuji, H.; Li, X.; Caricato, M.; Marenich, A. V.; Bloino, J.; Janesko, B. G.; Gomperts, R.; Mennucci, B.; Hratchian, H. P.; Ortiz, J. V.; Izmaylov, A. F.; Sonnenberg, J. L.; Williams-Young, D.; Ding, F.; Lipparini, F.; Egidi, F.; Goings, J.; Peng, B.; Petrone, A.; Henderson, T.; Ranasinghe, D.; Zakrzewski, V. G.; Gao, J.; Rega, N.; Zheng, G.; Liang, W.; Hada, M.; Ehara, M.; Toyota, K.; Fukuda, R.; Hasegawa, J.; Ishida, M.; Nakajima, T.; Honda, Y.; Kitao, O.; Nakai, H.; Vreven, T.; Throssell, K.; Montgomery, J. A., Jr.; Peralta, J. E.; Ogliaro, F.; Bearpark, M. J.; Heyd, J. J.; Brothers, E. N.; Kudin, K. N.; Staroverov, V. N.; Keith, T. A.; Kobayashi, R.; Normand, J.; Raghavachari, K.; Rendell, A. P.; Burant, J. C.; Iyengar, S. S.; Tomasi, J.; Cossi, M.; Millam, J. M.; Klene, M.; Adamo, C.; Cammi, R.; Ochterski, J. W.; Martin, R. L.; Morokuma, K.; Farkas, O.; Foresman, J. B.; Fox, D. J. *Gaussian 16*, Revision B.01, 2016.
(33) Singh, U. C.; Kollman, P. A. An Approach to Computing Electrostatic Charges for Molecules. *J. Comput. Chem.* **1984**, *5*, 129−145.
(34) Salomon-Ferrer, R.; Case, D. A.; Walker, R. C. An Overview of the Amber Biomolecular Simulation Package. *Wiley Interdiscip. Rev.: Comput. Mol. Sci.* **2013**, *3*, 198−210.
(35) Dupradeau, F.-Y.; Cezard, C.; Lelong, R.; Stanislawiak, E.; Pecher, J.; Delepine, J. C.; Cieplak, P. R.E.DD.B.: A database for RESP and ESP atomic charges, and force field libraries. *Nucleic Acids Res.* **2007**, *36*, D360−D367.
(36) Jorgensen, W. L.; Chandrasekhar, J.; Madura, J. D.; Impey, R. W.; Klein, M. L. Comparison of Simple Potential Functions for Simulating Liquid Water. *J. Chem. Phys.* **1983**, *79*, 926−935.
(37) Duan, Y.; Wu, C.; Chowdhury, S.; Lee, M. C.; Xiong, G.; Zhang, W.; Yang, R.; Cieplak, P.; Luo, R.; Lee, T.; Caldwell, J.; Wang, J.; Kollman, P. A Point-Charge Force Field for Molecular Mechanics Simulations of Proteins Based on Condensed-Phase Quantum Mechanical Calculations. *J. Comput. Chem.* **2003**, *24*, 1999−2012.
(38) Grest, G. S.; Kremer, K. Molecular Dynamics Simulation for Polymers in the Presence of a Heat Bath. *Phys. Rev. A: At., Mol., Opt. Phys.* **1986**, *33*, 3628−3631.
(39) Warshel, A.; Levitt, M. Theoretical Studies of Enzymic Reactions: Dielectric, Electrostatic and Steric Stabilization of the Carbonium Ion in the Reaction of Lysozyme. *J. Mol. Biol.* **1976**, *103*, 227−249.
(40) Field, M. J.; Albe, M.; Bret, C. l.; Proust-De Martin, F.; Thomas, A. The Dynamo Library for Molecular Simulations Using Hybrid Quantum Mechanical and Molecular Mechanical Potentials. *J. Comput. Chem.* **2000**, *21*, 1088−1100.
(41) Krzemińska, A.; Paneth, P.; Moliner, V.; Świderek, K. Binding Isotope Effects as a Tool for Distinguishing Hydrophobic and Hydrophilic Binding Sites of HIV-1 RT. *J. Phys. Chem. B* **2015**, *119*, 917−927.
(42) Field, M. J.; Bash, P. A.; Karplus, M. A Combined Quantum Mechanical and Molecular Mechanical Potential for Molecular Dynamics Simulations. *J. Comput. Chem.* **1990**, *11*, 700−733.
(43) Torrie, G. M.; Valleau, J. P. Nonphysical Sampling Distributions in Monte Carlo Free-Energy Estimation: Umbrella Sampling. *J. Comput. Phys.* **1977**, *23*, 187−199.
(44) Kumar, S.; Rosenberg, J. M.; Bouzida, D.; Swendsen, R. H.; Kollman, P. A. THE Weighted Histogram Analysis Method for Free-Energy Calculations on Biomolecules. I. The Method. *J. Comput. Chem.* **1992**, *13*, 1011−1021.
(45) Martí, S.; Moliner, V.; Tuñón, I. Improving the QM/MM Description of Chemical Processes: A Dual Level Strategy To Explore the Potential Energy Surface in Very Large Systems. *J. Chem. Theory Comput.* **2005**, *1*, 1008−1016.
(46) Ruiz-Pernía, J. J.; Silla, E.; Tuñón, I.; Martí, S.; Moliner, V. Hybrid QM/MM Potentials of Mean Force with Interpolated Corrections. *J. Phys. Chem. B* **2004**, *108*, 8427−8433.
(47) Baker, J.; Kessi, A.; Delley, B. The Generation and Use of Delocalized Internal Coordinates in Geometry Optimization. *J. Chem. Phys.* **1996**, *105*, 192−212.
(48) Samuel, G.; Laidler Keith, J. E. H. *The Theory of Rate Processes: The Kinetics of I Chemical Reactions, Viscosity, Diffusion and Electrochemical Phenomena*; Mcgraw-Hill Book Compagny: New York, 1941.
(49) Keck, J. C. Variational Theory of Reaction Rates. In *Advances in Chemical Physics*; Prigogine, I., Ed.; John Wiley & Sons, Inc.: Hoboken, NJ, USA, 2007; pp 85−121.
(50) Truhlar, D. G.; Garrett, B. C.; Klippenstein, S. J. Current Status of Transition-State Theory. *J. Phys. Chem.* **1996**, *100*, 12771−12800.
(51) Świderek, K.; Arafet, K.; Kohen, A.; Moliner, V. Benchmarking Quantum Mechanics/Molecular Mechanics (QM/MM) Methods on the Thymidylate Synthase-Catalyzed Hydride Transfer. *J. Chem. Theory Comput.* **2017**, *13*, 1375−1388.
(52) Krzemińska, A.; Moliner, V.; Świderek, K. Dynamic and Electrostatic Effects on the Reaction Catalyzed by HIV-1 Protease. *J. Am. Chem. Soc.* **2016**, *138*, 16283−16298.
(53) Świderek, K.; Kohen, A.; Moliner, V. The Influence of Active Site Conformations on the Hydride Transfer Step of the Thymidylate Synthase Reaction Mechanism. *Phys. Chem. Chem. Phys.* **2015**, *17*, 30793−30804.
(54) Wigner, E. Crossing of Potential Thresholds in Chemical Reactions. *Z. Phys. Chem.* **1932**, *B19*, 203−216.
(55) Truhlar, D. G.; Garrett, B. C. Variational Transition State Theory in the Treatment of Hydrogen Transfer Reactions. In *Hydrogen-Transfer Reactions*; John Wiley & Sons, Ltd, 2006; pp 833−874.
(56) Świderek, K.; Paneth, P. Binding Isotope Effects. *Chem. Rev.* **2013**, *113*, 7851−7879.
(57) Rohman, A.; van Oosterwijk, N.; Dijkstra, B. W. Purification, crystallization and preliminary X-ray crystallographic analysis of 3-ketosteroid Δ1-dehydrogenase fromRhodococcus erythropolisSQ1. *Acta Crystallogr., Sect. F: Struct. Biol. Cryst. Commun.* **2012**, *68*, 551−556.
(58) Eaton, J. W.; Bateman, D.; Hauberg, S.; Wehbring, R. *A High-Level Interactive Language for Numerical Computations*, GNU Octave Version 5.2.0 Manual, 2020.
(59) Johnson, K. A. Fitting Enzyme Kinetic Data with KinTek Global Kinetic Explorer. *Methods Enzymol.* **2009**, *467*, 601−626.
(60) Prinz, H. *Numerical Methods for the Life Scientist: Binding and Enzyme Kinetics Calculated with GNU Octave and MATLAB*; Springer-Verlag Berlin Heidelberg: Berlin, 2011.
(61) Glanowski, M.; Wójcik, P.; Procner, M.; Borowski, T.; Lupa, D.; Mielczarek, P.; Oszajca, M.; Świderek, K.; Moliner, V.; Bojarski, A. J.; Szaleniec, M. *Enzymatic Δ1-Dehydrogenation of 3-Ketosteroids—Reconciliation of Kinetic Isotope Effects with the Reaction Mechanism*; Mendeley Data, 2021.
(62) Rugor, A.; Wójcik-Augustyn, A.; Niedzialkowska, E.; Mordalski, S.; Staroń, J.; Bojarski, A.; Szaleniec, M. Reaction mechanism of sterol hydroxylation by steroid C25 dehydrogenase - Homology model, reactivity and isoenzymatic diversity. *J. Inorg. Biochem.* **2017**, *173*, 28−43.
(63) Melander, L. Evaluation of Rate-Constant Ratios from Experimental Data. *Isotope Effect on Reaction Rates*; The Ronald Press Company: New York, 1960; pp 46−64.
(64) Pérez Galende, P.; Hidalgo Cuadrado, N.; Kostetsky, E. Y.; Roig, M. G.; Villar, E.; Shnyrov, V. L.; Kennedy, J. F. Kinetics of Spanish broom peroxidase obeys a Ping-Pong Bi-Bi mechanism with competitive inhibition by substrates. *Int. J. Biol. Macromol.* **2015**, *81*, 1005−1011.

https://doi.org/10.1021/acscatal.1c01479
ACS Catal. 2021, 11, 8211−8225

(65) Singh, D.; Chaudhury, S. Single-Molecule Kinetics of an Enzyme in the Presence of Multiple Substrates. *ChemBioChem* **2018**, *19*, 842−850.
(66) Cleland, W. W. The Kinetics of Enzyme-Catalyzed Reactions with Two or More Substrates or Products. *Biochim. Biophys. Acta, Spec. Sect. Enzymol. Subj.* **1963**, *67*, 188−196.
(67) Burnham, K. P.; Anderson, D. R. Multimodel Inference: Understanding AIC and BIC in Model Selection. *Socio. Methods Res.* **2004**, *33*, 261−304.
(68) Gadda, G.; Sobrado, P. Kinetic Solvent Viscosity Effects as Probes for Studying the Mechanisms of Enzyme Action. *Biochemistry* **2018**, *57*, 3445−3453.
(69) Valley, M. P.; Fitzpatrick, P. F. Reductive Half-Reaction of Nitroalkane Oxidase: Effect of Mutation of the Active Site Aspartate to Glutamate†,‡. *Biochemistry* **2003**, *42*, 5850−5856.
(70) Fafarman, A. T.; Sigala, P. A.; Schwans, J. P.; Fenn, T. D.; Herschlag, D.; Boxer, S. G. Quantitative, Directional Measurement of Electric Field Heterogeneity in the Active Site of Ketosteroid Isomerase. *Proc. Natl. Acad. Sci. U.S.A.* **2012**, *109*, E299−E308.

https://doi.org/10.1021/acscatal.1c01479
ACS Catal. 2021, 11, 8211−8225